Emulation of two-dimensional photonic crystal defect modes in a photonic crystal with a three-dimensional photonic band gap

M. L. Povinelli, Steven G. Johnson, Shanhui Fan, and J. D. Joannopoulos
Department of Physics and the Center for Materials Science and Engineering, Massachusetts Institute of Technology, 77 Massachusetts Avenue, Cambridge, Massachusetts 02139
(Received 30 January 2001; published 27 July 2001)

Using numerical simulations, we demonstrate the construction of two-dimensional- (2D-) like defect modes in a recently proposed 3D photonic crystal structure. These modes, which are confined in all three dimensions by a complete photonic band gap, bear a striking similarity to those in 2D photonic crystals in terms of polarization, field profile, and projected band structures. It is expected that these results will greatly facilitate the observation of widely studied 2D photonic-crystal phenomena in a realistic, 3D physical system.

DOI: 10.1103/PhysRevB.64.075313 PACS number(s): 42.70.Qs

I. INTRODUCTION

Photonic crystals, periodic dielectric structures that can prohibit light propagation in a range of wavelengths,[1–3] have been the subject of intense research in the last decade.[4] One particularly interesting aspect of these systems is the possibility of creating crystal defects that confine light in localized modes. Advances in understanding of these defect modes have stimulated the design of photonic-crystal waveguides, resonant cavities, filters, and other practical optical components, leading toward the possibility of integrated optical circuits.[5]

Much of the theoretical investigation of photonic crystals has been carried out in two-dimensional (2D) systems, due to the inherent simplicity of calculation, visualization, and understanding in 2D. Many interesting and potentially useful physical phenomena have been discovered in 2D, including high transmission through sharp bends in photonic-crystal waveguides,[6] channel-drop tunneling through localized states,[7,8] high localization in microcavities,[9] elimination of cross talk in waveguides,[10] and high transmission in wide-angle splitters.[11] Fortunately these phenomena are based on general principles that are not restricted to two dimensions, for experimental realization requires the use of three-dimensional structures.

In order to achieve three-dimensional confinement, two general types of three-dimensional photonic-crystal system have been proposed. One type is photonic-crystal slabs, two-dimensionally periodic structures of finite height. In these structures, light is confined by a combination of an in-plane photonic band gap and out-of-plane index guiding.[12,13] While it is possible to create localized linear-[14–20] and point-[21–23] defect modes in slab systems, the lack of a complete band gap is an inherent limitation that results in radiation losses in all cases where the translational symmetry of the crystal is destroyed, for example, in waveguide bends.[18] A second type of system, three-dimensionally periodic photonic crystals with a complete band gap, has no such theoretical limitation. The complex geometry of most three-dimensional crystals, however, makes the study and understanding of defects in these systems more difficult; the modes typically cannot be approximated by their simpler, well understood, two-dimensional analogs.

Recently, a structure and method of fabrication were proposed for a 3D photonic crystal with a large, complete band gap.[24] This structure is composed of alternating layers of triangular lattices of air rods in dielectric and dielectric rods in air; cross sections thus correspond to 2D photonic-crystal geometries. In this paper, we discuss how this feature, in combination with the large band gap, greatly simplifies the understanding of defect modes. We show that line- and point-defect modes of the full, 3D photonic crystal have a close correspondence in band structure, field profile, and polarization to the modes of the respective 2D photonic-crystal geometries.

Moreover, the 3D photonic crystal structure that we study here allows the combination of line- and point-defect modes in a similar manner to that which is possible in 2D photonic crystals.[25,26] Thus, these results promise that two-dimensional analyses and phenomena, even in complex integrated optical devices, may be directly applicable to a three-dimensional crystal with an omnidirectional band gap, with only slight changes in parameters and the resulting mode characters.

II. CRYSTAL STRUCTURE

The 3D photonic-crystal structure of interest is shown in Fig. 1(a). The arrows indicate the two different types of layer that make up the structure. Fig. 1(b) shows horizontal cross sections through these layers. Layer I has the form of a triangular lattice of dielectric rods in air; we refer to it as a *rod layer*. Layer II has the form of a triangular lattice of air holes in dielectric; we refer to it as a *hole layer*. (The shape of the rods is a result of a proposed fabrication method, and is not essential for the properties of the crystal.[24]) The underlying lattice of the photonic crystal is face-centered cubic (fcc). Centers of the holes are placed at fcc lattice sites, and hole and rod layers are stacked along the [111] direction.

It was shown in Ref. 24 that this structure has a large, complete band gap of around 20% of the midgap frequency for Si/air structures with suitable choices for the structural parameters. Lengths may be specified in terms of $\bar{a}$, the nearest-neighbor spacing within either a hole or rod layer. The nearest-neighbor spacing is related to the fcc lattice constant a by $\bar{a}=a/\sqrt{2}$. For the calculations presented here, the hole radius is taken to be $r_h=0.414\bar{a}$. The radius of a cylin-

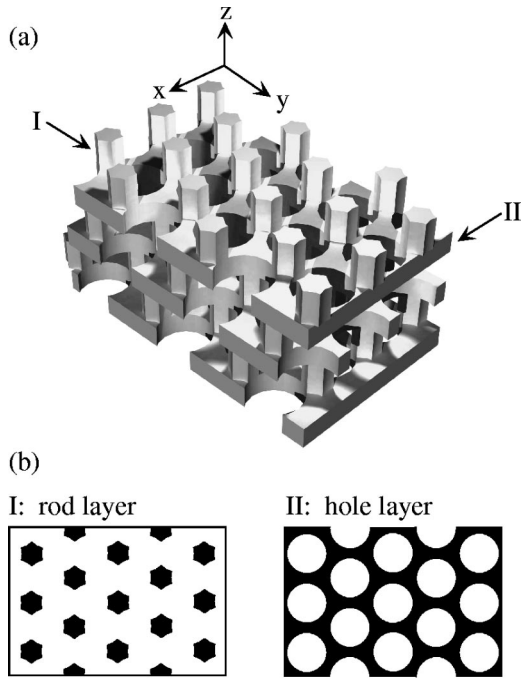

FIG. 1. (a) Computer rendering of the 3D photonic-crystal structure studied in this work. The structure consists of two alternating types of layer, indicated by the arrows. We refer to the type of layer labeled I as a rod layer, and that labeled II as a hole layer. (b) Cross sections of rod and hole layers. These cross sections have the same geometry as the two types of widely studied 2D photonic crystal: arrays of dielectric rods in air and arrays of air holes in dielectric.

drical rod with the same area as a rod in the structure is $r_r = 0.175\bar{a}$. The thickness of a hole layer is $0.318\bar{a}$, and the thickness of a rod layer is $0.500\bar{a}$. These values correspond to an optimal parameter set that maximizes the gap size,[24] where the dielectric constant of the high-index material is taken to be $\epsilon = 12$.

It is particularly significant for the present work that cross sections of hole and rod layers have the same geometry as the two widely studied, canonical 2D photonic-crystal structures: an array of air holes in dielectric, which supports a TE gap and TE defect modes, and an array of dielectric cylinders in air, which supports a TM gap and TM defect modes. We will show here that this geometrical feature, in combination with the presence of a 3D photonic band gap, allows us to construct 2D-like defect modes in the 3D structure.

III. COMPUTATIONAL METHODS

The computational methods used to calculate photonic band structures and electromagnetic field modes employ preconditioned conjugate-gradient minimization of the Rayleigh quotient in a plane-wave basis and are described in detail elsewhere.[27] A supercell method was used for defect calculations: the defect was surrounded by several periods of the unperturbed crystal within a ''supercell,'' and periodic boundary conditions were applied. The supercell dimensions were chosen to be large enough for adjacent waveguides/cavities to have minimal effect on mode frequencies and fields. Projected bands corresponding to bulk modes were computed using a defect-free supercell.

IV. LINEAR-DEFECT MODES

It is well known that linear defects in photonic crystals can act as waveguides.[3] These defects can be created by either adding or removing high-index material, altering the effective index of the waveguide in comparison to its surroundings. However, it is the reduced-index case that is unique to photonic crystals. Traditional dielectric waveguides, which operate on the principle of index guiding, necessarily confine light to regions of higher index. In contrast, photonic-crystal waveguides can guide light in regions of lower index, even primarily in air. We focus here on reduced-index linear-defect modes.

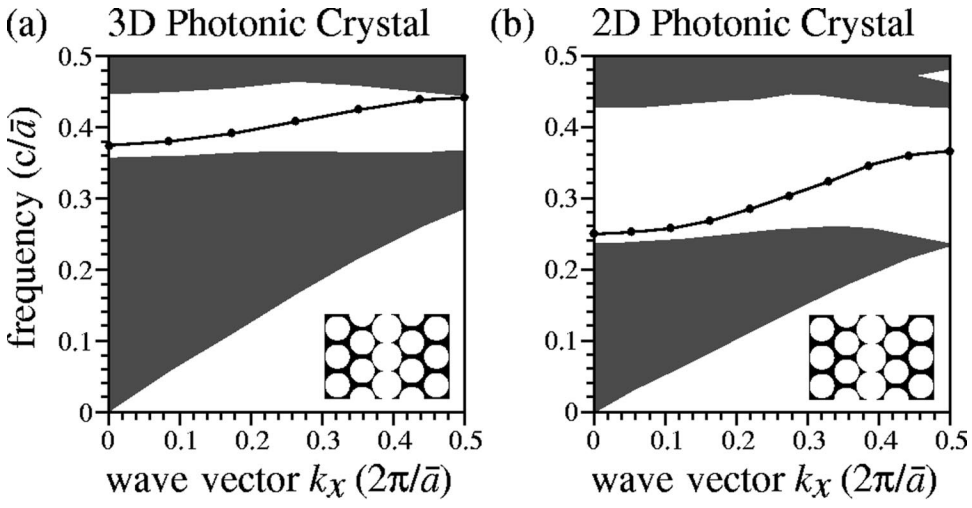

FIG. 2. (a) Projected band structure for the 3D crystal with a linear defect created by altering a single hole layer. Shown in the inset is a horizontal cross section through the midplane of the defect (parallel to the x-y plane). The radius of the defect holes is $r_h' = 0.500\bar{a}$, as compared to $r_h = 0.414\bar{a}$ in the bulk, where $\bar{a}$ is the in-plane distance between nearest-neighbor holes. (b) Projected band structure for the TE modes of the 2D crystal with identical geometry to the cross section of the 3D crystal shown in Fig. 2(a).

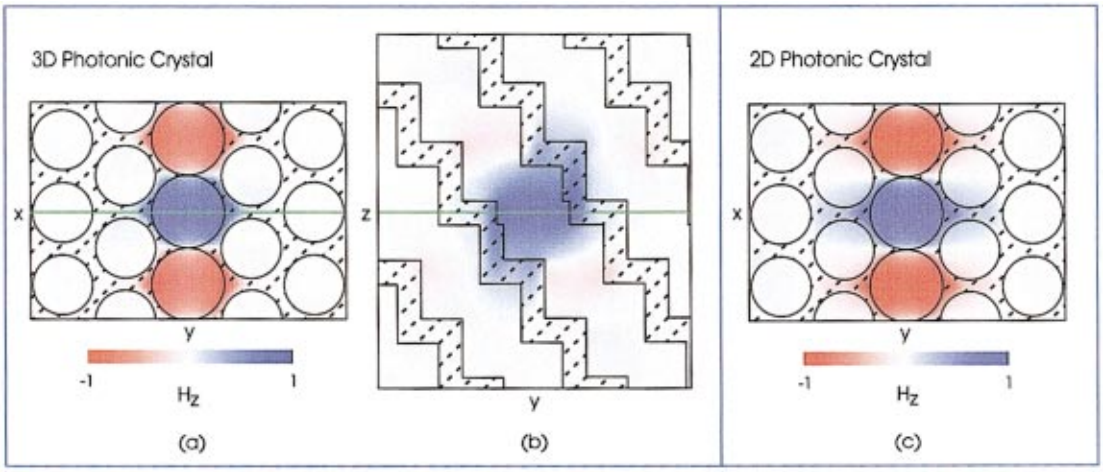

FIG. 3. (Color) Mode profiles for the increased-hole linear-defect states from Fig. 2 at the Brillouin zone edge. Overlaid crosshatches indicate regions of high dielectric material. (a),(b) The field for the 3D linear-defect structure corresponding to Fig. 2(a). H_z is plotted for horizontal and vertical cross sections of the 3D crystal. The cross sections intersect along the green lines on the figures. (c) H_z for the 2D linear-defect structure shown in the inset to Fig. 2(b).

We first consider the case where a *single hole layer* of the 3D photonic crystal is modified to create a linear defect. As we will show, this has the effect of introducing a TE-like mode into the hole layer. To create a reduced-index linear defect, we increased the radii of a line of nearest-neighbor holes from $r_h = 0.414\bar{a}$ to $r_h' = 0.500\bar{a}$. At this value, the holes just touch. A horizontal cross section of the structure, through the center of the defect, is shown in the inset to Fig. 2(a). Notice that the geometry of this cross section is identical to that of a 2D line defect in a 2D structure of air holes in dielectric, as shown in the inset to Fig. 2(b).

The projected band structure, or dispersion diagram, for the 3D line-defect structure is shown in Fig. 2(a) and compared with that for the 2D line-defect structure in Fig. 2(b). Shaded regions indicate extended states in the perfect crystal. The frequencies of these states are plotted as a function of k_x, the component of the wave vector along the direction of the linear defect, which takes on values between 0 and $\pi/\bar{a}$. For the 3D structure, *all* modes are projected onto the band diagram and the structure has a large, complete band gap. For the 2D structure, only TE modes are shown, since it is for the TE polarization that a large gap is present. Moreover, only modes with wave vectors corresponding to in-plane propagation are considered in calculating the 2D dispersion relation. In both Figs. 2(a) and 2(b), the line within the gap region shows the dispersion relation of the single-mode defect band. The states within this band are confined to the region of the defect. For the 3D case, the band extends from a lower frequency of $0.37c/\bar{a}$ to an upper frequency of $0.44c/\bar{a}$. In the 2D case, the band extends from $0.25c/\bar{a}$ to $0.37c/\bar{a}$. The similarities between the 3D and 2D projected band structures are notable. In both cases, a *single* defect band extends across the entire Brillouin zone, inside the band gap. The shapes of the defect bands are also similar, since both bands must exhibit vanishing group velocity at both the center and edge of the Brillouin zone.

In addition to the resemblance between the projected band structures, there is a strong, quantifiable similarity between the defect modes in the 3D and 2D crystals. Figures 3(a) and 3(b) show the field profiles for the 3D defect state at the edge of the Brillouin zone for horizontal and vertical cross sections through the center of the linear defect. (The horizontal cross section is parallel to the x-y plane, and the vertical cross section is parallel to the y-z plane.) In both cases, the z component of the H field is shown. The green lines on the figures indicate the intersection of these cross sections. The 3D defect mode is, clearly, strongly localized near the defect in all three dimensions. Figure 3(c) shows the magnetic field for the 2D defect state at the same k point.

Comparing the horizontal cross section of the 3D defect mode to that of to the 2D defect mode, we see that the two

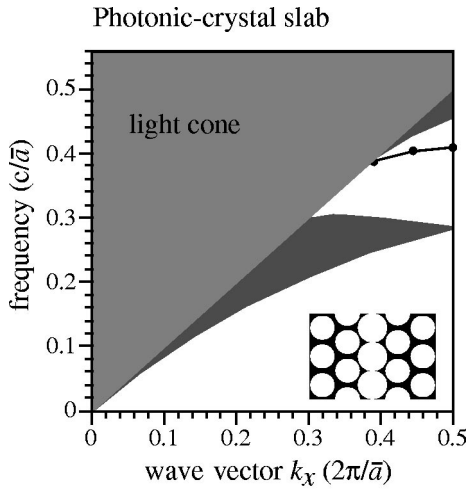

FIG. 4. Projected band structure for a photonic-crystal slab, with a linear defect as in Fig. 2. A cross section of the slab is shown in the inset; the thickness of the slab is $0.71\bar{a}$. The light-gray region indicates the light cone; dark gray regions indicate even-symmetry modes of the bulk structure.

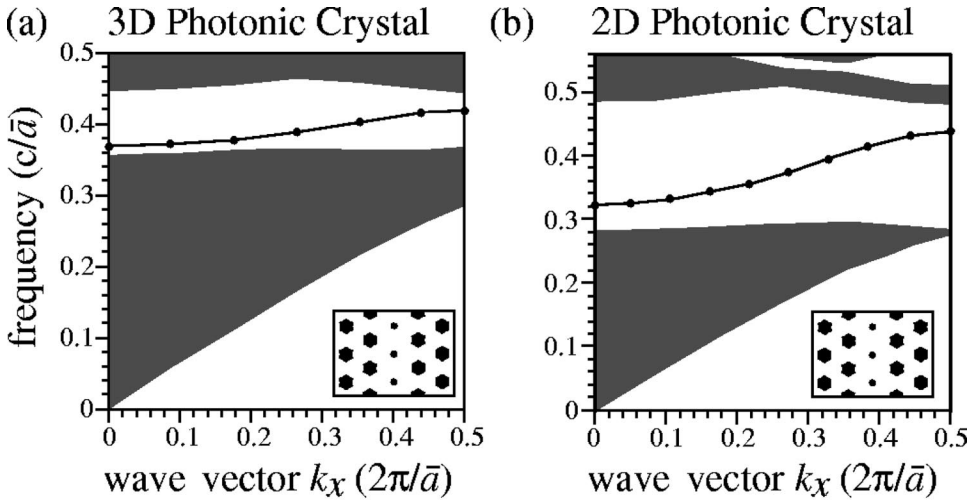

FIG. 5. (a) Projected band structure for the 3D crystal with a linear defect created by altering a single rod layer. A row of nearest-neighbor rods has been replaced with cylindrical rods of radius $r_r' = 0.07\bar{a}$. Shown in the inset is a horizontal cross section through the midplane of the defect. (b) Projected band structure for the TM modes of the corresponding 2D photonic crystal.

are nearly identical in polarization and profile; we quantify this observation in the following. In the 2D crystal, the continuous translational invariance of the crystal in the z direction allows a separation of the electromagnetic field modes into TE and TM polarizations. The defect mode in Fig. 3(c) is purely TE polarized; the H field is entirely in the z direction. In the 3D crystal, the horizontal plane through the center of the defect is not a mirror plane of the 3D structure. Thus symmetry considerations do not require the defect mode to be purely TE or TM polarized there. However, we observe that the 3D mode is nearly TE polarized in this plane:

$$R_H \equiv \frac{\int d^2r\, |\mathbf{H}_z^{3D}(\omega;\mathbf{r})|^2}{\sum_j \int d^2r\, |H_j^{3D}(\omega;\mathbf{r})|^2} \approx 0.98, \tag{1}$$

where the integral is taken over the horizontal plane. The similarity of the mode profiles may also be quantified, by computing an overlap between the horizontal cross sections of the 3D state and the 2D state. For the states shown in Fig. 3,

$$O_H \equiv \left| \frac{\int d^2r\, \mathbf{H}^{3D}(\omega,\mathbf{r})^* \cdot \mathbf{H}^{2D}(\omega,\mathbf{r})}{\sqrt{\int d^2r\, |\mathbf{H}^{3D}(\omega,\mathbf{r})|^2 \int d^2r\, |\mathbf{H}^{2D}(\omega,\mathbf{r})|^2}} \right|^2 \approx 0.94. \tag{2}$$

The similarity between the mode profiles is a consequence of the localization of the 3D defect mode to a 2D-like environment, and relies on the presence of a large, complete band gap in a 3D structure with 2D-like cross sections.

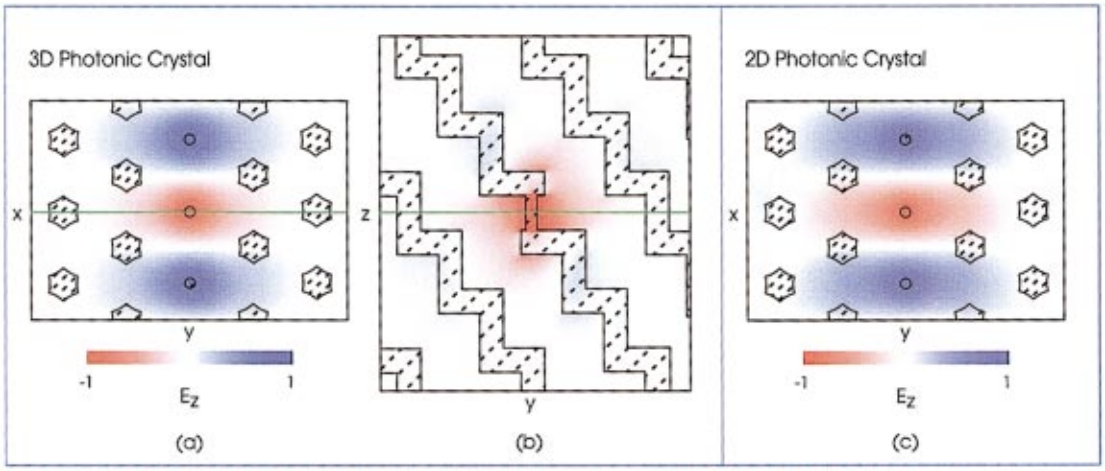

FIG. 6. (Color) Mode profiles for the reduced-rod linear-defect states from Fig. 5 at the Brillouin zone edge. (a,b) The field for the 3D linear-defect structure corresponding to Fig. 5(a). E_z is plotted for horizontal and vertical cross sections of the 3D structure. (c) The field for the 2D structure shown in Fig. 5(b).

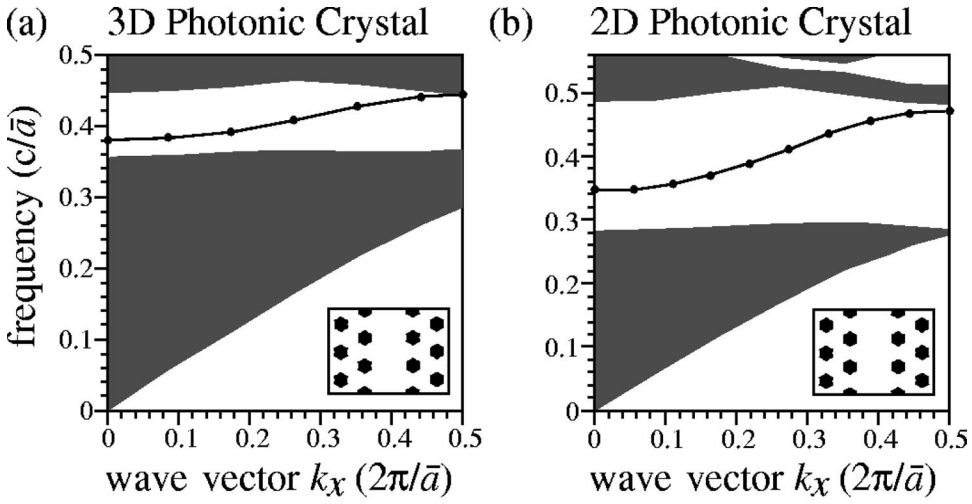

FIG. 7. (a) Projected band structure for the 3D crystal with a linear defect created by removing a row of nearest-neighbor rods in a single rod layer. Shown in the inset is a cross section through the midplane of the defect. (b) Projected band structure for the TM modes of the corresponding 2D photonic crystal.

Previous work has studied linear defect modes in photonic-crystal slabs,[18] which can also have a strong resemblance to the defect modes of two-dimensional photonic crystals. However, it is important to stress that the projected band structures of photonic-crystal slabs and two-dimensional photonic crystals are very different. Figure 4 shows the projected band structure for a slab with the same cross section as the 3D and 2D structures considered above. The thickness of the slab was taken to be $0.71\bar{a}$, which approximately optimizes the gap size.[13] The light-gray region indicates the light cone, a continuum of all possible frequencies of the bulk background, in this case air. The dark-gray regions indicate the even-symmetry bulk modes of the slab. The region of k space covered by neither the bulk modes nor the light cone is only a fraction of the Brillouin zone, sharply limiting the bandwidth of the guided mode. This is in sharp contrast to the projected band structures for the 3D and 2D photonic crystals shown in Fig. 2, where the gap extends across the entire Brillouin zone.

We have shown that a TE-like defect mode can be introduced into the 3D photonic crystal by altering a hole layer. A TM-like defect mode can similarly be created by modifying a rod layer of the structure. This was done by replacing a row of nearest-neighbor rods with smaller, cylindrical rods of radius $r_r' = 0.071\bar{a}$. The projected band structure for the 3D photonic crystal is shown in Fig. 5(a), and a cross section through the linear defect is shown in the inset. Figure 5(b) shows the projected band structure for the TM modes of the 2D photonic crystal with the corresponding geometry. Again the band structures are quite similar, with a single-mode defect band extending across the entire Brillouin zone.

Mode profiles for 3D and 2D defect states at the Brillouin zone edge are shown in Fig. 6. Figures 6(a) and 6(b) show the z component of the E field for the 3D defect mode. The

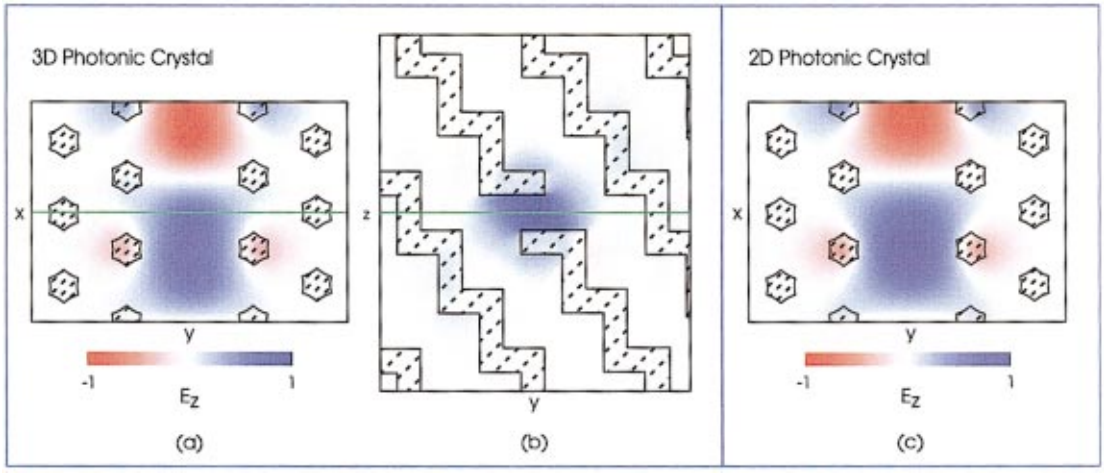

FIG. 8. (Color) Mode profiles for the removed-rod linear-defect state at $k_x = 0.265(2\pi/\bar{a})$. (a,b) The field for the 3D linear-defect structure corresponding to Fig. 7(a). E_z is plotted for horizontal and vertical cross sections of the 3D structure. (c) The field for the 2D structure shown in Fig. 7(b).

2D defect mode is shown in Fig. 6(c) and is TM polarized (the E field is entirely in the z direction). The 3D defect mode is nearly TM polarized, with

$$R_E \equiv \frac{\int d^2r\,|E_z(\omega;\mathbf{r})|^2}{\sum_j \int d^2r\,|E_j(\omega;\mathbf{r})|^2} \approx 0.99. \tag{3}$$

The mode profiles are again very similar; in order to define a suitable overlap function, it is necessary to consider the orthonormality properties of the E field. Suppose that $\mathbf{E}_1(\omega,\mathbf{r})$ and $\mathbf{E}_2(\omega,\mathbf{r})$ are the electric fields corresponding to two eigenmodes of a fixed 2D dielectric structure specified by $\epsilon(\mathbf{r})$. It follows from Maxwell's equations that although $\mathbf{E}_1$ and $\mathbf{E}_2$ are not orthonormal under the usual metric it is true that

$$\int d^2r\,\epsilon(\mathbf{r})\,\mathbf{E}_1(\omega,\mathbf{r})^* \cdot \mathbf{E}_2(\omega,\mathbf{r}) = 0. \tag{4}$$

It is thus sensible to compute an overlap of the 3D and 2D defect modes by

$$O_E \equiv \left| \frac{\int d^2r\,\epsilon(\mathbf{r})\,\mathbf{E}^{3D}(\omega,\mathbf{r})^* \cdot \mathbf{E}^{2D}(\omega,\mathbf{r})}{\sqrt{\int d^2r\,\epsilon(\mathbf{r})\,|\mathbf{E}^{3D}(\omega,\mathbf{r})|^2 \int d^2r\,\epsilon(\mathbf{r})\,|\mathbf{E}^{2D}(\omega,\mathbf{r})|^2}} \right|^2; \tag{5}$$

the value was found to be approximately 0.95.

A reduced-index linear defect can also be created by completely removing a line of rods. The resulting 3D and 2D band structures are shown in Fig. 7. The single-mode defect band in the 3D structure approaches the bulk states at the edge of the Brillouin zone. The perpendicular E field for $k_x = 0.265(2\pi/\bar{a})$ is shown in Fig. 8. As in the case of the reduced-radius rods, the 2D mode is completely TM polarized and the 3D defect mode is nearly TM polarized, with $R_E \approx 0.99$; the overlap $O_E \approx 0.98$. We note that the possibility of creating a guided mode by completely removing rods in a photonic-crystal *slab* is much more limited, since the necessity of vertical index guiding does not allow truly guided modes that reside mainly in air.[18] This is illustrated in Fig. 9, which shows the projected band structure for a rod slab of thickness $2\bar{a}$. There is at most a very weakly confined defect mode very close to the edge of the band gap.

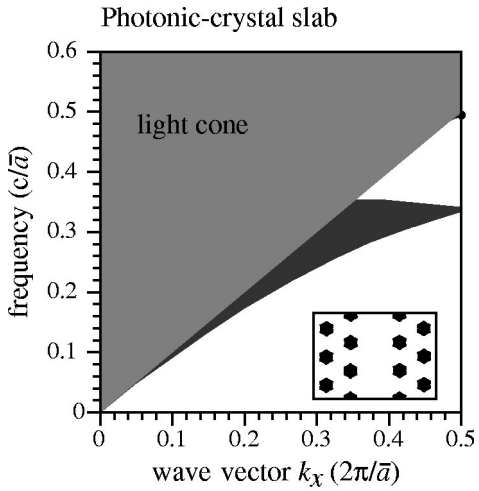

FIG. 9. Projected band structure for a photonic-crystal slab, with a linear defect as in Fig. 8. A cross section of the slab is shown in the inset; the thickness of the slab is $2\bar{a}$. The light-gray region indicates the light cone; dark-gray regions indicate odd-symmetry modes of the bulk structure. In contrast to Fig. 4, there is at most a very weakly guided defect mode very near the edge of the band gap.

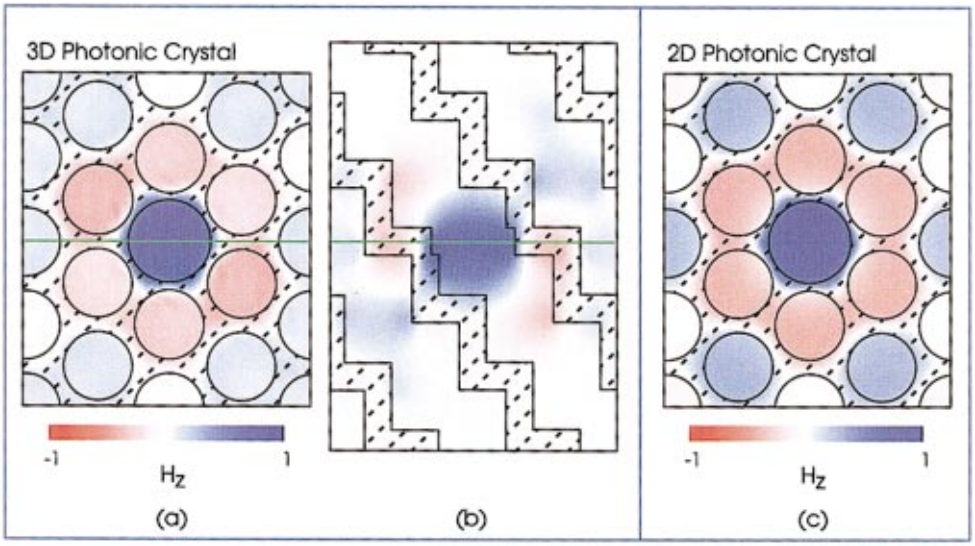

FIG. 10. (Color) (a,b) Defect-mode profile for a point defect in the 3D crystal created by increasing the radius of a hole in a single hole layer to $r_h' = 0.500\bar{a}$. H_z is plotted for horizontal and vertical cross sections of the 3D crystal. (c) Defect-mode profile for the corresponding 2D crystal.

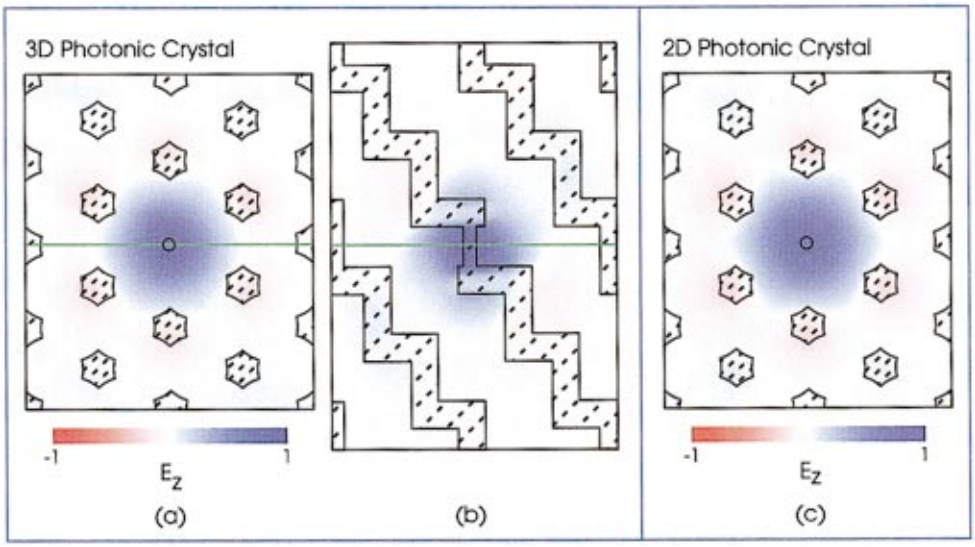

FIG. 11. (Color) (a,b) Defect-mode profile for a point defect in the 3D crystal created by reducing the radius of a rod in a single rod layer to $r_r' = 0.071\bar{a}$. E_z is plotted for horizontal and vertical cross sections of the 3D crystal. (c) Defect-mode profile for the corresponding 2D crystal.

For all three cases of reduced-index waveguides in the 3D crystal, a single-mode, defect-state band is obtained within the complete, three-dimensional band gap. The waveguide modes are strongly localized within the altered layer, and both the projected band structures and midplane field profiles of the three-dimensional structures are very similar to those of the corresponding two-dimensional photonic crystals.

V. POINT-DEFECT MODES

In the previous section, reduced-index *linear* defects were created in the 3D photonic crystal structure by altering either the hole or rod layer. Reduced-index *point* defects can be created in a similar manner. In Figs. 10, 11, and 12, we compare the point-defect modes in the 3D structure with those in the corresponding 2D structure. As for linear defects, the mode profiles and polarization are very similar in the two structures.

Figure 10 shows the perpendicular H field for a hole defect, where the defect radius was taken to be $r_h' = 0.500\bar{a}$. The 3D mode has a frequency of $0.40c/\bar{a}$, which falls near the middle of the band gap $(0.36-0.44)c/\bar{a}$. It is strongly localized in all three dimensions to the vicinity of the point defect. Moreover, it is nearly TE polarized in the midplane, with $R_H \approx 0.98$. The 2D mode has a frequency of $0.28c/\bar{a}$, where the band gap runs over the frequency range $(0.26-0.43)c/\bar{a}$. The overlap of the 3D and 2D point-defect modes is $O_H \approx 0.92$.

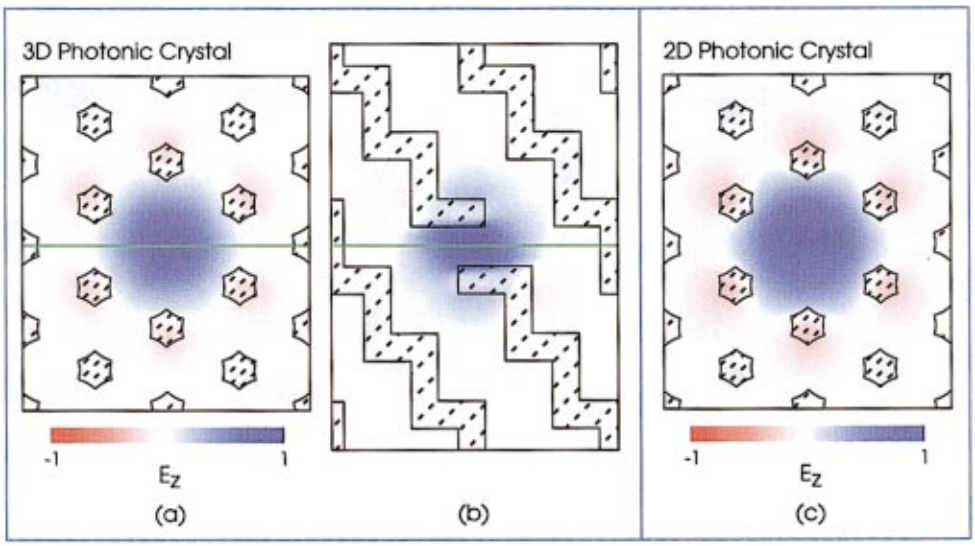

FIG. 12. (Color) (a,b) Defect-mode profile for a point defect in the 3D crystal created by removing a rod in a single rod layer. E_z is plotted for horizontal and vertical cross sections of the 3D crystal. (c) Defect-mode profile for the corresponding 2D crystal.

Rod defects are shown in Figs. 11 and 12. In Fig. 11, a single rod is replaced with a reduced-radius rod with $r_r' = 0.071\bar{a}$. The 3D defect mode, which has a frequency of $0.40c/\bar{a}$, falls in the middle of the band gap $(0.36-0.44)c/\bar{a}$. The 2D defect mode has a frequency of $0.37c/\bar{a}$, with a band gap range of $(0.30-0.48)c/\bar{a}$. In Fig. 12, a rod is completely removed. The defect mode frequencies are $0.41c/\bar{a}$ as compared to a gap range of $(0.36-0.44)c/\bar{a}$ for the 3D structure and $0.41c/\bar{a}$ as compared to a gap range of $(0.30-0.48)c/\bar{a}$ for the 2D structure. In both cases, the 3D defect modes are nearly TM polarized ($R_E \approx 0.99$) while the 2D defect modes are completely TM polarized. The overlaps between the 3D and corresponding 2D modes are again high, with $O_E \approx 0.97$ for both cases.

VI. CONCLUSION

We have studied linear- and point-defect modes in a recently proposed 3D photonic crystal with a complete band gap. The cross sections of the 3D crystal have the geometry of a 2D photonic crystal, allowing comparison between the two systems. The mode polarization, mode profile, and projected band structures of defect modes in the 3D crystal are very similar to those for the corresponding 2D crystal.

Promising directions for future work include the study of physical phenomena previously observed only in two-dimensional photonic crystals, and the design of components for integrated optical circuits within this realistic, three-dimensional system.

ACKNOWLEDGMENT

This work was supported in part by the Materials Research Science and Engineering Center program of the National Science Foundation under Award No. DMR-9400334.

[1] E. Yablonovitch, Phys. Rev. Lett. **58**, 2059 (1987).
[2] S. John, Phys. Rev. Lett. **58**, 2486 (1987).
[3] J. D. Joannopoulos, R. D. Meade, and J. N. Winn, *Photonic Crystals* (Princeton University Press, Princeton, NJ, 1995).
[4] For an overview of recent work, see, e.g., *Photonic Crystals and Light Localization*, edited by C. M. Soukoulis, Proceedings of the NATO Advanced Study Institute on Photonic Band Gap Materials, Limin Hersonissou, Crete, 2000 (Kluwer Academic, Dordrecht, 2001).
[5] J. D. Joannopoulos, P. R. Villeneuve, and S. Fan, Nature (London) **386**, 143 (1997).
[6] A. Mekis, J. C. Chen, I. Kurland, S. Fan, P. R. Villeneuve, and J. D. Joannopoulos, Phys. Rev. Lett. **77**, 3787 (1996).
[7] S. Fan, P. R. Villeneuve, J. D. Joannopoulos, and H. A. Haus, Phys. Rev. Lett. **80**, 960 (1998).
[8] S. Fan, P. R. Villeneuve, J. D. Joannopoulos, M. J. Khan, C. Manolatou, and H. A. Haus, Phys. Rev. B **59**, 15 882 (1999).
[9] P. R. Villeneuve, S. Fan, and J. D. Joannopoulos, Phys. Rev. B **54**, 7837 (1996).
[10] S. G. Johnson, C. Manolatou, S. Fan, P. R. Villeneuve, J. D. Joannopoulos, and H. A. Haus, Opt. Lett. **23**, 1855 (1998).
[11] S. Fan, S. G. Johnson, J. D. Joannopoulos, C. Manolatou, and H. A. Haus, J. Opt. Soc. Am. B **18**, 162 (2001).
[12] R. D. Meade, A. Devenyi, J. D. Joannopoulos, O. L. Alerhand, D. A. Smith, and K. Kash, J. Appl. Phys. **75**, 4753 (1994).
[13] S. G. Johnson, S. Fan, P. R. Villeneuve, J. D. Joannopoulos, and L. A. Kolodziejski, Phys. Rev. B **60**, 5751 (1999).
[14] S. Kuchinsky, D. C. Allan, N. F. Borrelli, and J.-C. Cotteverte, Opt. Commun. **175**, 147 (2000).
[15] T. Søndergaard, A. Bjarklev, M. Kristensen, J. Erland, and J. Broeng, Appl. Phys. Lett. **77**, 785 (2000).
[16] A. Chutinan and S. Noda, Phys. Rev. B **62**, 4488 (2000).
[17] S. Y. Lin, E. Chow, S. G. Johnson, and J. D. Joannopoulos, Opt. Lett. **25**, 1297 (2000).
[18] S. G. Johnson, P. R. Villeneuve, S. Fan, and J. D. Joannopoulos, Phys. Rev. B **62**, 8212 (2000).
[19] M. Loncar, T. Doll, J. Vučković, and A. Scherer, J. Lightwave Technol. **18**, 1402 (2000).
[20] H.-Y. Ryu, J.-K. Hwang, and Y.-H. Lee, J. Appl. Phys. **88**, 4941 (2000).
[21] P. R. Villeneuve, S. Fan, S. G. Johnson, and J. D. Joannopoulos, IEE Proc.: Optoelectron. **145**, 384 (1998).
[22] R. Coccioli, M. Boroditsky, K. W. Kim, Y. Rahmat-Samii, and E. Yablonovitch, IEE Proc.: Optoelectron. **145**, 391 (1998).
[23] R. K. Lee, O. Painter, B. Kitzke, A. Scherer, and A. Yariv, J. Opt. Soc. Am. B **17**, 629 (2000).
[24] S. G. Johnson and J. D. Joannopoulos, Appl. Phys. Lett. **77**, 3490 (2000).
[25] M. Agio, E. Lidorikis, and C. M. Soukoulis, J. Opt. Soc. Am. B **17**, 2037 (2000).
[26] C. J. M. Smith, T. F. Krauss, H. Benisty, M. Rattier, C. Weisbuch, U. Oesterle, and R. Houdré, J. Opt. Soc. Am. B **17**, 2043 (2000).
[27] See, e.g., R. D. Meade, A. M. Rappe, K. D. Brommer, J. D. Joannopoulos, and O. L. Alerhand, Phys. Rev. B **48**, 8434 (1993); S. G. Johnson, *ibid.* **55**, 15 942(E) (1997); and most recently S. G. Johnson and J. D. Joannopoulos, Opt. Express **8**, 173 (2001).